ChemComm

Cite this: *Chem. Commun.*, 2011, **47**, 12792–12794

www.rsc.org/chemcomm

COMMUNICATION

Highly active Pt@Au nanoparticles encapsulated in perfluorosulfonic acid for the reduction of oxygen†

Niancai Cheng,[a] Huaiguang Li,[a] Guoqiang Li,[b] Haifeng Lv,[a] Shichun Mu,*[a] Xueliang Sun[c] and Mu Pan[a]

Received 22nd August 2011, Accepted 25th October 2011
DOI: 10.1039/c1cc15203c

The Pt@Au catalysts demonstrate remarkably high oxygen reduction reaction (ORR) activity compared with Pt/C catalysts. The ORR of $Pt_2@Au_1/C$ and $Pt_1@Au_2/C$ is 9.5 and 6.6 times that of Pt/C, respectively. This improvement is attributed to the electronic structure effect of the Au core on the Pt shell and introduction of PFSA.

The widespread commercialization of low-temperature polymer electrolyte membrane (PEM) fuel cells is severely hampered by several issues, including the low catalytic activity and high cost of Pt-based catalysts for the oxygen reduction reaction (ORR) at the cathode.[1] To overcome these barriers, on the one hand researchers have been looking for other alternative materials to replace the Pt-based catalysts,[2] on the other hand they have engineered the morphology or composition of Pt-based catalysts to maximize their activity.[3] For example, a Pt-based alloy with other transition metals demonstrated enhanced electrocatalytic activity for the ORR.[4] However, the dissolution of non-noble metals from these catalysts can influence catalyst activity and contaminate the electrode membrane,[4e,5] leading to a decrease in the PEM fuel cell performance. Fortunately, core–shell structure catalysts such as Pt@Ni can alleviate this problem because the Pt shell can protect the non-noble metal core.[6] Nevertheless, non-noble alloying materials are still not stable and can diffuse onto the Pt nanoparticle surface in the acidic environment of a PEM fuel cell, at highly positive cathodic potentials.[5,7]

Recently Pt@Au catalysts have attracted attention because Pt@Au catalysts have higher activity for oxygen reduction and higher stability compared with pure Pt catalysts.[8] This enhanced activity for oxygen reduction is attributed to the strain and ligand effect of the core substrate on the noble metal shell.[9] In this study, we introduce a novel Pt@Au nanoparticle catalyst encapsulated in perfluorosulfonic acid (PFSA) that shows remarkably high activity for the ORR (Scheme 1). In this novel system, the PFSA not only acts as a stabilizer for the Pt@Au catalyst, but it also enhances the activity of Pt@Au catalysts on the electrode of a PEM fuel cell because PFSA, or Nafion, is conventionally impregnated into the catalyst layers of the PEM fuel cells in the form of a recast film and improves the activity of the Pt catalyst and increases proton conductivity. In addition, using PFSA to encapsulate the surface of the novel Pt@Au catalyst can improve the lifetime of the Pt/C catalyst because of a stabilization effect.[10]

Scheme 1 illustrates the approach used to synthesize the Pt@Au nanoparticles. Using PFSA (Nafion) as a nanoparticle stabilizer is important for controlling the size and monodispersity of both the Au seed and the Pt@Au nanoparticles at every step.[8a] The size of the Au seed was controlled by adjusting the ratio of Nafion to metal, and the Pt layer thickness and surface coverage on the Au seed changed with the ratio of atomic Pt/Au (Scheme 1b and c). Energy dispersive X-ray analysis (EDX) studies of individual metal nanoparticles revealed the presence of the elements C, F and S on the metal nanoparticles, most likely derived from the Nafion layers on the outer surface of the metal nanoparticles.[10]

The UV-Vis absorption spectra from an aqueous suspension of Au nanoparticles and Pt@Au hydrosols are shown in Fig. S1, ESI.† The Au spectrum has a peak at 517 nm due to the surface plasma resonance property of Au; however, this peak disappears in the spectrum from the Pt@Au hydrosol, indicating that the

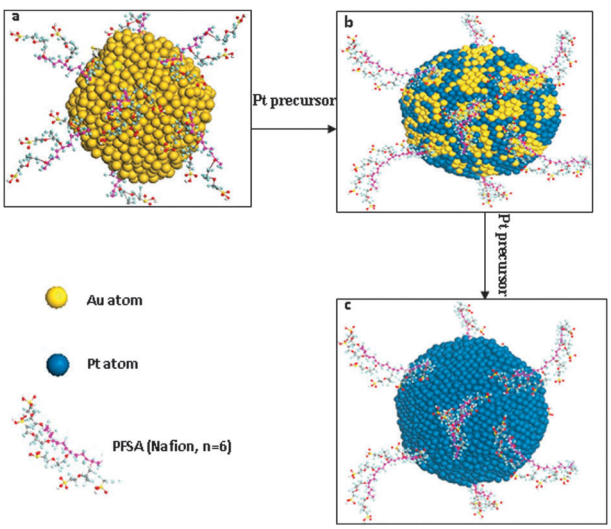

Scheme 1 Schematic diagram of the synthesis of Pt@Au nanoparticles.

[a] *State Key Laboratory of Advanced Technology for Materials Synthesis and Processing, Wuhan University of Technology, 430070, China. E-mail: msc@whut.edu.cn*
[b] *College for Materials Science and Engineering, South China University of Technology, 381 Wushan, Guangzhou 510641, China*
[c] *Department of Mechanical and Materials Engineering, University of Western Ontario, London, Ontario N6A 5B9, Canada*

† Electronic supplementary information (ESI) available: Catalyst synthesis and characterization; Table S1; Fig. S1–S5. See DOI: 10.1039/c1cc15203c

Pt atoms almost completely cover the surface of the Au nanoparticles. The size of the Au nanoparticles was approximately 4.4 nm. The Pt shell thickness was calculated according to the reported formula[11] (see Table S1, ESI†), and it increased as the Pt to Au atomic ratio increased. The Pt shell thickness of $Pt_1@Au_2$ nanoparticles was 0.31 nm, which is slightly larger than the Pt atomic diameter of 0.278 nm.[12] Therefore, we believe that a complete monolayer of Pt atoms was formed on the surface of the Au core with the successive and tunable reduction method. As the Pt to Au atomic ratio increased, the Pt shell thickness of $Pt_4@Au_1$ nanoparticles increased to 1.58 nm, which is approximately five layers of Pt atoms. The Pt@Au nanoparticles were also characterized using transmission electron microscopy (TEM) (see Fig. S2, ESI†). All the synthesized nanoparticles were well dispersed without aggregation and had a narrow size distribution due to the stabilizing effect of the PFSA. The average size (as measured by TEM analysis) of the nanoparticles made from different Pt to Au atomic ratios is in agreement with the calculated values as listed in Table S1, ESI.† The Pt@Au nanoparticles made with different Pt to Au ratios were uniform within each ratio group and the size of the Pt@Au nanoparticles increased with increasing Pt to Au ratio.

Further characterization with high-resolution transmission electron microscopy (HRTEM) was conducted to examine the core–shell structure of the Pt@Au nanoparticles. A typical TEM image of the $Pt_1@Au_1$ nanoparticles is shown in Fig. 1A, with a magnified TEM image shown in Fig. 1B. Fig. 1C is an enlargement of one of the particles seen in Fig. 1B, and the lattice fringes can be seen very clearly. Fig. 1D is a Fourier transform of the image seen in Fig. 1B and provides more detailed structural information on these particles. A face-centered cubic (fcc) structure is seen in the zone axis, and the corresponding plane indices are labeled. This result is expected given the fcc structure seen for both Au and Pt elements. The weak diffraction spots seen in Fig. 1D could originate from the very small image area used for the Fourier transform or the different lattice spacing of Au and Pt. The lattice parameters of Au and Pt are 0.4078 and 0.3924 nm, respectively. This small difference is not enough to generate two sets of diffraction patterns, though it can cause an observable broadening of the diffraction spots. In Fig. 1B, we notice that the spacing between the central atoms (0.350 nm) is larger than those on the outskirts (0.340 nm). The former is close to the Au [−11−1] spacing of 0.353 nm, suggesting the presence of a Au core, and the latter is exactly the same as the value for Pt along its [−11−1] direction, indicating the existence of a Pt shell covering the particle. An intensity profile along the [−11−1] direction of the particle, indicated by a line in Fig. 1C, is shown in Fig. 1E. The experimental value for the Au inter-atomic spacing is slightly smaller than the theoretical value, which is due to the effect of the Pt shell whose atomic spacing is smaller than the Au core.

Fig. S3, ESI† shows the cyclic voltammograms (CVs) for Pt@Au/C catalysts in deaerated 0.1 mol dm^{-3} $HClO_4$ with a glass carbon electrode. The electrochemically active surface area (ECSA) was calculated based on the hydrogen adsorption peak area in the CVs. For all the Pt@Au/C catalysts, the Au core was completely covered with Pt because the characteristic Au reduction peak at 1.05 V *vs.* RHE[13] was noticeably absent, which is consistent with the UV-Vis absorbance data. The ECSA was calculated to be 183, 110, 71, 48 m^2 g^{-1}_{Pt} for Pt to

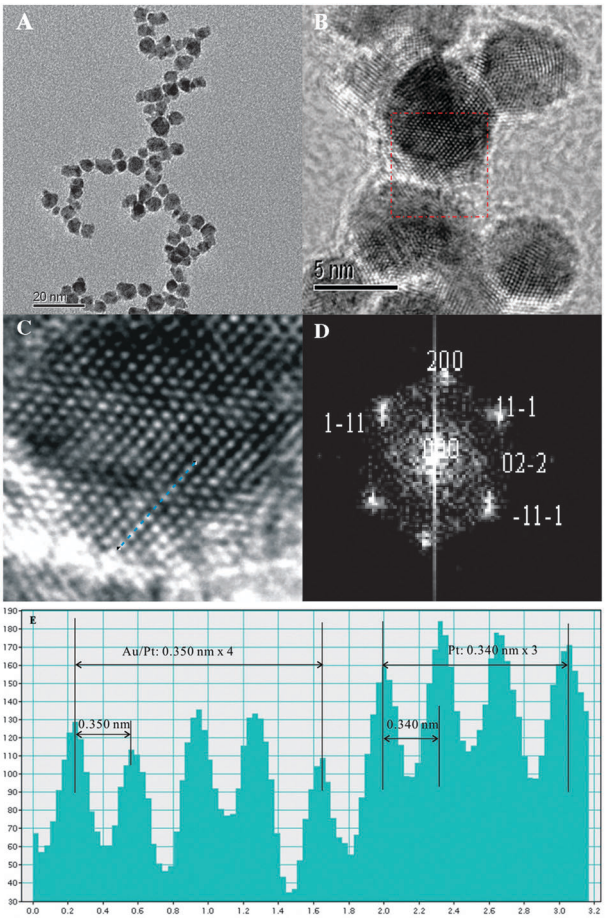

Fig. 1 (A) TEM image of $Pt_1@Au_1$ nanoparticles. (B) HRTEM image of $Pt_1@Au_1$ nanoparticles. (C) An enlargement of a particle in Fig. 1B as indicated by the red square. (D) An FFT transform of Fig. 1B, showing that the zone axis is [011], with the plane indices clearly labeled. (E) Intensity profile along the line in Fig. 1B, where the spacing difference between atoms can be seen. The unit for the *x*-axis is nm.

Au atomic ratios of 1 : 2, 1 : 1, 2 : 1 and 4 : 1, respectively. The metal mass-specific activities are 61, 55, 47, 39 m^2 $g^{-1}_{(Pt+Au)}$ for Pt to Au atomic ratios of 1 : 2, 1 : 1, 2 : 1 and 4 : 1, respectively. Clearly, the catalytic activity of Pt@Au catalysts with atomic ratios of Pt to Au of 1 : 2 and 1 : 1 is significantly improved compared to that of Pt/C catalysts (Johnson Matthey), which have an ECSA of 70 m^2 g^{-1}_{Pt} (Fig. S3B, ESI†). The Pt ECSA for $Pt_1@Au_2/C$ and $Pt_1@Au_1/C$ catalysts are 2.6 times and 1.5 times that of Pt/C catalysts, respectively. Upon increasing the Pt to Au ratio, the ECSA of Pt@Au/C catalysts significantly decreased due to the thicker Pt shell and larger particle size (Fig. S3B, ESI†). In addition, the potentials for Pt oxide formation and reduction shift positively with Pt@Au/C catalysts compared with Pt/C catalysts. This shift is due to the interaction between the Pt shell and Au core,[8d] which probably induces higher ORR activity in the catalysts.[14]

Fig. 2 compares the polarization curves for the ORR in Pt/C catalysts and Pt@Au/C catalysts with different Pt to Au ratios. The measurements were performed in an oxygen-saturated 0.1 mol dm^{-3} $HClO_4$ solution with a glassy carbon rotating disk electrode as the working electrode. All Pt@Au/C catalysts exhibited higher ORR activity than Pt/C catalysts. At 0.85 V *vs.* RHE, the Pt mass activities of ORR in Pt@Au/C catalysts were

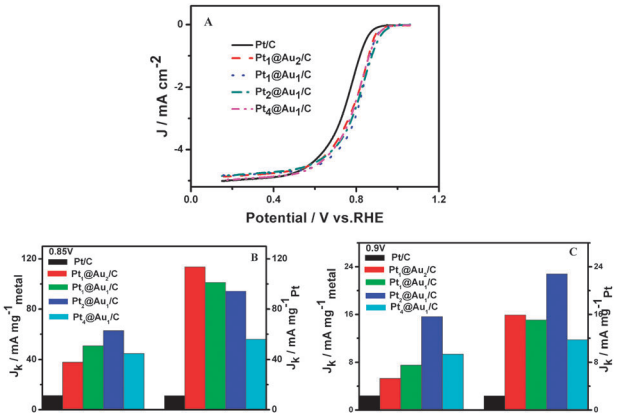

Fig. 2 (A) Comparison of the ORR activities of the commercial Pt/C and Pt@Au/C catalysts in 0.1 mol dm^{-3} $HClO_4$ for ORR at 2500 rpm, a sweep rate of 5 mV s^{-1} with scanning the potential in the negative direction and at room temperature. Pt mass activity and total noble metal mass activity of different electrocatalysts at (B) 0.85 V and (C) 0.90 V *vs.* RHE.

113.61, 101.22, 94.25 and 55.95 mA mg^{-1}_{Pt} for Pt to Au atomic ratios of 1 : 2, 1 : 1, 2 : 1 and 4 : 1, respectively, while the Pt mass activity of ORR in Pt/C catalysts is only 11.23 mA mg^{-1}_{Pt}. The ORR activities of $Pt_1@Au_2/C$ catalysts with Pt to Au atomic ratios of 1 : 2, 1 : 1, 2 : 1 and 4 : 1 were 10.1, 9.0, 8.3 and 4.9 times that of the Pt/C catalyst (Fig. 2B), respectively. At 0.90 V *vs.* RHE, the Pt mass activity of ORR for Pt@Au/C catalysts was 15.9, 15.06, 22.8 and 11.72 mA mg^{-1}_{Pt} for Pt to Au atomic ratios of 1 : 2, 1 : 1, 2 : 1 and 4 : 1, and these values were 6.6, 6.3, 9.5 and 4.9 times that of the Pt/C catalysts (2.39 mA mg^{-1}_{Pt}), respectively (Fig. 2C). For the total metal mass activity, Pt@Au/C catalysts also have better activity than that of Pt/C catalysts. And the $Pt_2@Au_1/C$ have highest total metal mass activity at 0.85 and 0.90 V *vs.* RHE (Fig. 2B and C). The remarkably higher activity of ORR in the Pt@Au/C catalysts is primarily attributed to the electronic structure effect (strain and ligand effects) of the Au core on the Pt shell.[8d,9] X-Ray diffraction data (see Fig. S4, ESI†) showed that the Pt@Au/C catalysts display certain negative shifts in the diffraction peak as compared to Pt/C catalysts, which confirms the electronic structure effect of the Au core on the Pt shell. In addition, the improvement in ORR activity partly comes from the presence of the SO^-_3 end groups in Nafion, which can enhance and facilitate the transfer process for reactive species involved in the ORR (see Fig. S5, ESI†).

In summary, we have synthesized Pt@Au nanoparticles using the successive and tunable reduction method, and investigated the core–shell structure of the nanoparticles. The Pt@Au catalysts have shown a remarkable enhancement in ORR compared with Pt/C catalysts, with ORR activities of $Pt_2@Au_1/C$ and $Pt_1@Au_2/C$ catalysts of 9.5 and 6.6 times, respectively, that of the Pt/C catalysts. This enhanced ORR activity is attributed to the electronic structure effect (strain and ligand effects) of the Au core on the Pt shell, as well as the presence of SO^-_3 end groups in Nafion, which can enhance and facilitate the transfer process of reactive species involved in the ORR. This novel core–shell structure catalyst allows for the development of next-generation catalysts with high ORR activity and low amounts of Pt, with the potential for many applications beyond fuel cells.

This work was supported by the National Natural Science Foundation of China (NSFC) (50972112) and the Major State Basic Research Development Program of China (973 Program) (No.2012CB215504).

Notes and references

1 (*a*) T. Ghosh, M. B. Vukmirovic, F. J. DiSalvo and R. R. Adzic, *J. Am. Chem. Soc.*, 2010, **132**, 906–907; (*b*) Y. Zhang, Q. H. Huang, Z. Q. Zou, J. F. Yang, W. Vogel and H. Yang, *J. Phys. Chem. C*, 2010, **114**, 6860–6868; (*c*) J. Greeley, I. E. L. Stephens, A. S. Bondarenko, T. P. Johansson, H. A. Hansen, T. F. Jaramillo, J. Rossmeisl, I. Chorkendorff and J. K. Norskov, *Nat. Chem.*, 2009, **1**, 552–556.
2 R. McGuire, D. K. Dogutan, T. S. Teets, J. Suntivich, Y. Shao-Horn and D. G. Nocera, *Chem. Sci.*, 2010, **1**, 411–414.
3 B. Lim, M. J. Jiang, P. H. C. Camargo, E. C. Cho, J. Tao, X. M. Lu, Y. M. Zhu and Y. A. Xia, *Science*, 2009, **324**, 1302–1305.
4 (*a*) L. Xiong and A. Manthiram, *J. Electrochem. Soc.*, 2005, **152**, A697–A703; (*b*) G. X. Wang, H. M. Wu, D. Wexler, H. K. Liu and O. Savadogo, *J. Alloys Compd.*, 2010, **503**, L1–L4; (*c*) V. R. Stamenkovic, B. S. Mun, M. Arenz, K. J. J. Mayrhofer, C. A. Lucas, G. F. Wang, P. N. Ross and N. M. Markovic, *Nat. Mater.*, 2007, **6**, 241–247; (*d*) Y. Y. Feng, J. H. Ma, G. R. Zhang, G. Liu and B. Q. Xu, *Electrochem. Commun.*, 2010, **12**, 1191–1194; (*e*) S. Chen, P. J. Ferreira, W. C. Sheng, N. Yabuuchi, L. F. Allard and Y. Shao-Horn, *J. Am. Chem. Soc.*, 2008, **130**, 13818–13819.
5 K. J. J. Mayrhofer, K. Hartl, V. Juhart and M. Arenz, *J. Am. Chem. Soc.*, 2009, **131**, 16348–16349.
6 J. Zhang, F. H. B. Lima, M. H. Shao, K. Sasaki, J. X. Wang, J. Hanson and R. R. Adzic, *J. Phys. Chem. B*, 2005, **109**, 22701–22704.
7 R. Borup, J. Meyers, B. Pivovar, Y. S. Kim, R. Mukundan, N. Garland, D. Myers, M. Wilson, F. Garzon, D. Wood, P. Zelenay, K. More, K. Stroh, T. Zawodzinski, J. Boncella, J. E. McGrath, M. Inaba, K. Miyatake, M. Hori, K. Ota, Z. Ogumi, S. Miyata, A. Nishikata, Z. Siroma, Y. Uchimoto, K. Yasuda, K. I. Kimijima and N. Iwashita, *Chem. Rev.*, 2007, **107**, 3904–3951.
8 (*a*) J. Luo, L. Wang, D. Mott, P. N. Njoki, Y. Lin, T. He, Z. Xu, B. N. Wanjana, I. I. S. Lim and C. J. Zhong, *Adv. Mater.*, 2008, **20**, 4342–4347; (*b*) N. Kristian and X. Wang, *Electrochem. Commun.*, 2008, **10**, 12–15; (*c*) Y. W. Ma, H. M. Zhang, H. X. Zhong, T. Xu, H. Jin and X. Y. Geng, *Catal. Commun.*, 2010, **11**, 434–437; (*d*) J. F. Zhai, M. H. Huang and S. J. Dong, *Electroanalysis*, 2007, **19**, 506–509; (*e*) D. F. Yancey, E. V. Carino and R. M. Crooks, *J. Am. Chem. Soc.*, 2010, **132**, 10988–10989.
9 (*a*) J. R. Kitchin, J. K. Norskov, M. A. Barteau and J. G. Chen, *J. Chem. Phys.*, 2004, **120**, 10240–10246; (*b*) V. R. Stamenkovic, B. Fowler, B. S. Mun, G. F. Wang, P. N. Ross, C. A. Lucas and N. M. Markovic, *Science*, 2007, **315**, 493–497; (*c*) P. Strasser, S. Koh, T. Anniyev, J. Greeley, K. More, C. F. Yu, Z. C. Liu, S. Kaya, D. Nordlund, H. Ogasawara, M. F. Toney and A. Nilsson, *Nat. Chem.*, 2010, **2**, 454–460.
10 N. C. Cheng, S. C. Mu, M. Pan and P. P. Edwards, *Electrochem. Commun.*, 2009, **11**, 1610–1614.
11 A. Henglein, *J. Phys. Chem. B*, 2000, **104**, 2201–2203.
12 X. W. Li, J. Y. Liu, W. He, Q. H. Huang and H. Yang, *J. Colloid Interface Sci.*, 2010, **344**, 132–136.
13 K. Hartl, K. J. J. Mayrhofer, M. Lopez, D. Goia and M. Arenz, *Electrochem. Commun.*, 2010, **12**, 1487–1489.
14 H. R. Colon-Mercado and B. N. Popov, *J. Power Sources*, 2006, **155**, 253–263.

